Progress In Electromagnetics Research C, Vol. 74, 161–170, 2017

Dual-Sense Dual-Polarized Hybrid Rectangular Dielectric Resonator Antenna for Multiband Applications

Nikesh K. Sahu, Anand Sharma, and Ravi K. Gangwar*

Abstract—In this communication, a dual-sense dual-polarized hybrid rectangular dielectric resonator antenna (RDRA) is explored. Two leading aims of the present article include: (i) to obtain dual-polarization characteristics, i.e., the combination of linear and circular polarizations; (ii) to achieve quad-band features by using the concept of hybrid antenna. Modified printed line is used to excite dual radiating modes in RDRA, i.e., $\mathrm{TE}^{x}_{\delta 11}$ and $\mathrm{TE}^{y}_{1\delta 1}$. In order to authenticate the proposed radiator, archetype of the proposed antenna is fabricated and tested. Good accord is established between measured and simulated outcomes. The proposed radiator is operated over four different frequency bands, i.e., 1.81 GHz–2.06 GHz, 2.37 GHz–2.7 GHz, 3.35 GHz–4.4 GHz, and 4.62 GHz–5.62 GHz. Left Hand Circularly Polarized (LHCP) and Right Hand Circularly Polarized (RHCP) waves are obtained form 4.1–4.39 GHz and 4.78–5.2 GHz respectively. All these properties of the proposed radiator make it appropriate for 3G/WLAN/WiMAX applications.

1. INTRODUCTION

In recent era of wireless communication, it is required to have an antenna with low profile, light weight, high gain characteristics. In order to fulfill all these requirements, we have two different types of antennas: microstrip antenna and dielectric resonator antenna. Although microstrip antenna is able to fulfill all these requirements, it suffers from high metallic losses and low gain [1]. To overcome this drawback, dielectric resonator antenna comes into the picture with high gain and high radiation efficiency. There are three basic shapes available in dielectric resonator antenna: hemispherical, cylindrical and rectangular ones. Out of the three, rectangular shape is widely used because it has two degrees of freedom [2].

Two important antenna characteristics are required by the modern wireless communication, i.e., circular/dual-polarization characteristics and multiband characteristics. These radiators have a lot of advantages, such as capability to operate multiple operating bands, reducing multipath fading, and orientation insensitive. In open literature, there are three important methods available to create multiband features in dielectric resonator antenna, i.e., (i) grouping of DRA with other radiating elements, i.e., hybrid structure [3, 4]; (ii) grouping of DRA with resonating element which is not directly connected to feeding structure [5]; (iii) multiple mode excitation in DRA [6, 7]. Similarly, some of the research works have also been done in the area of dual-polarized/circularly polarized DRAs such as hybrid Z-shaped CDRA, aperture coupled RDRA, probefed CDRA and chamfered DRA, and rectangular DRA with square shaped slot [8–12].

In this article, a hybrid rectangular dielectric resonator antenna is presented. Square ring shaped monopole is used to originate two different frequency bands at 1.95 GHz and 5.09 GHz. An inverted L-shaped printed line is used to create orthogonal modes in RDRA, i.e., $TE^{x}_{\delta 11}$ and $\mathrm{TE}^{y}_{1\delta 1}$ and generates

Received 2 March 2017, Accepted 26 April 2017, Scheduled 31 May 2017

* Corresponding author: Ravi Kumar Gangwar (ravi.gangwar.ece07@itbhu.ac.in).
The authors are with the Department of Electronics Engineering, Indian Institute of Technology (Indian School of Mines), Dhanbad, Jharkhand 826004, India.

circularly polarized wave (CP wave) in the third frequency band. Similarly, CP wave in the fourth frequency band is created by an inverted L-strip. It is used to produce 90° phase shift between x-and y-polarized E-field lines of a square-shaped monopole. The proposed antenna structure is operated over four different frequency bands, i.e., 1.81–2.06 GHz, 2.37–2.7 GHz, 3.35–4.4 GHz and 4.62–5.62 GHz with a fractional bandwidth of 12.91%, 13.01%, 27.1%, and 19.53%, respectively. Section 2 and Section 3 of proposed article describe antenna formation and its analysis, respectively. Section 4 is focused on the experimental verification of the proposed antenna structure. Finally, conclusion is described in Section 5.

2. DESCRIPTION OF ANTENNA STRUCTURE AND MATHEMATICAL ANALYSIS

A schematic diagram of the proposed antenna structure is shown in Fig. 1. Modified square-shaped patch has been etched over an FR4 substrate ($\epsilon_{r,sub}$ = 4.4, $\tan\delta$= 0.02). The thickness of the FR-4 substrate is 1.6 mm. Rectangular DRA ($\varepsilon_{Alumina}$ = 9.8, $\tan\delta$ = 0.002) is fixed over the modified square-shaped patch with the help of glue (quick-fix). A prototype of the proposed antenna structure is displayed in Fig. 2. Dimensions of different optimized parameters are given in Table 1.

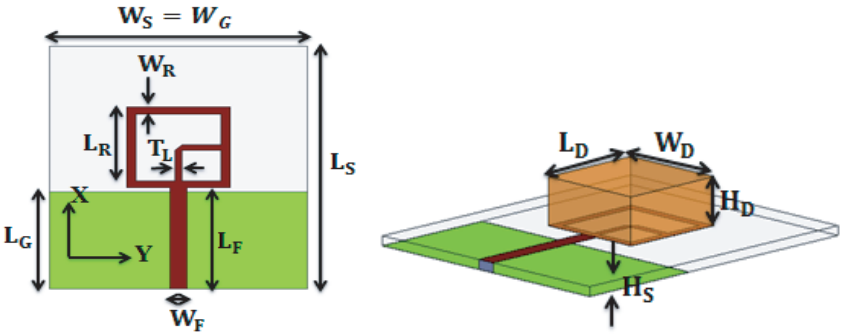

Figure 1. Graphical layout of proposed radiator. (a) Feeding mechanism. (b) 3D view.

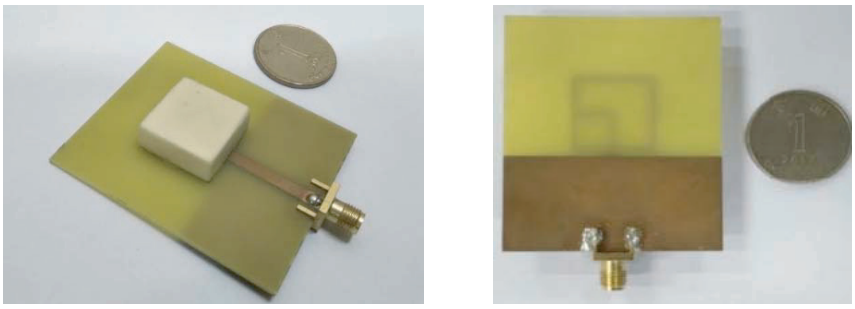

Figure 2. Fabricated picture of proposed radiator. (a) Isometric view. (b) Bottom view.

Theoretically, formula for calculating the resonant frequency of the square ring shape monopole is given as below [13]:

$$f_r = \frac{v_0}{4(L_R - W_R)\sqrt{\varepsilon_r}} \tag{1}$$

where, v_0 is the velocity of light in free space and ε_r the relative permittivity of substrate. L_R and W_R are the length and thickness of the square-shaped ring. It is important to note here that Eq. (1) is applicable when: (i) length of ring shaped monopole lies in between 10.0 mm to 30.0 mm; (ii) width

Table 1. Optimized antenna design parameters.

Design Parameters	Dimensions	Material Used
Substrate Length (L_S) Substrate Width (W_S) Substrate Height (H_S)	$L_S \times W_S \times H_S$ $60 \times 50 \times 1.6\,\text{mm}^3$	$FR4$ ($\epsilon_{r,sub} = 4.4$, $\tan(\delta) = 0.02$)
Dielectric Resonator Length (L_D) Dielectric Resonator Width (W_D) Dielectric Resonator Height (H_D)	$L_D \times W_D \times H_D$ $20 \times 20 \times 8\,\text{mm}^3$	Alumina ceramic ($\epsilon_{Alumina} = 9.8$, $\tan(\delta) = 0.002$)
Ground Plane Length (L_G) Ground Plane Width (W_G) Ground Plane Thickness (T_G)	$L_G \times W_G \times T_G$ $24 \times 50 \times 0.035\,\text{mm}^3$	Copper
Microstrip line Length (L_F) Microstrip line Width (W_F) Square ring Thickness(W_R) Square ring Length (L_R) Inverted L-shaped printed line thickness (T_L)	$L_F = 26.7\,\text{mm}$ $W_F = 3.4\,\text{mm}$ $T_R = 1.75\,\text{mm}$ $L_R = 20\,\text{mm}$ $T_L = 1.2\,\text{mm}$	Copper

of the ring lies in between 0.5 mm to 3.0 mm [13]. In the case of the proposed antenna, both conditions are fulfilled. From Eq. (1), the resonant frequency of the square-ring monopole is found to be 1.9 GHz.

There is no straight formula available for calculating the resonant frequency of fundamental modes in rectangular DRA, but we can predict its frequency with the help of dielectric waveguide model (DWM). The resonant frequency for $\text{TE}^x_{\delta 11}$ and $\text{TE}^y_{1\delta 1}$ modal fields can be predicted with reasonable accuracy as follow [14],

For $\text{TE}^x_{\delta 11}$ mode,

$$f_r = \frac{v_0}{2\pi\sqrt{\varepsilon_r}}\sqrt{k_x^2 + k_y^2 + k_z^2} \tag{2}$$

$$\text{where,} \quad k_y = \frac{\pi}{b}, \quad k_z = \frac{\pi}{d} \tag{3}$$

$$k_x \tan\left(k_x \frac{a}{2}\right) = \sqrt{(\varepsilon_r - 1)\, k_0^2 - k_x^2} \tag{4}$$

For $\text{TE}^y_{1\delta 1}$ mode,

$$f_r = \frac{v_0}{2\pi\sqrt{\varepsilon_r}}\sqrt{k_x^2 + k_y^2 + k_z^2} \tag{5}$$

$$\text{where,} \quad k_x = \frac{\pi}{a}, \quad k_z = \frac{\pi}{d} \tag{6}$$

$$k_y \tan\left(k_y \frac{b}{2}\right) = \sqrt{(\varepsilon_r - 1)\, k_0^2 - k_y^2} \tag{7}$$

where f_r is the resonant frequency, and k_x, k_y, and k_z are the wave numbers in the x, y, and z directions. v_0 is the velocity of light in free space, and a, b, d are the length, width, height of the rectangular DRA, respectively.

3. ANTENNA ANALYSIS

Investigation of the proposed radiator has been carried out by using Ansys HFSS EM simulator. This section is focused on understanding the phenomenon of generation of quad frequency bands and CP wave in proposed radiator.

3.1. Effect of Partial Ground Plane

Figure 3 displays the variation of reflection coefficient ($|S_{11}|$) with change in the length of ground surface. Two observations are found in Fig. 3: (i) Increment in the ground surface enhances the coupling between ground surface and radiator which in turn enhances capacitive effect. This makes the proposed radiator almost non-resonant. (ii) As the length of partial ground plane decreases, coupling between feed line and rectangular DRA decreases. It is because ring-shape patch behaves more as a radiator than a feed line [17]. Therefore, the optimized value for the length of ground surface is taken as 24 mm.

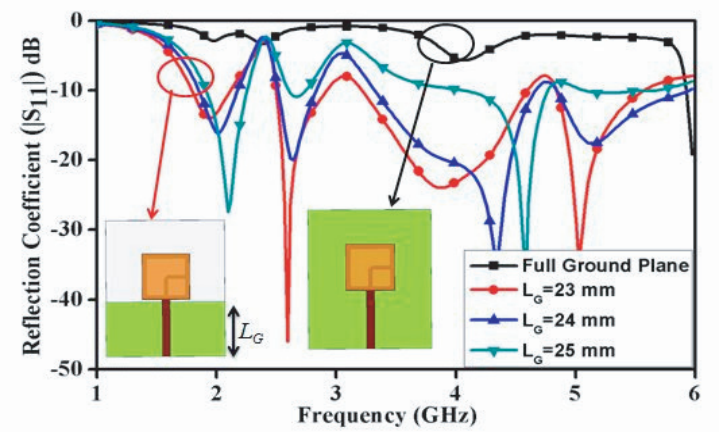

Figure 3. Variation in reflection coefficient characteristics with modification in ground surface length.

3.2. Outcome of Different Resonating Configurations

The reflection coefficient variation ($|S_{11}|$) with different resonating structures is shown in Fig. 4. It can be perceived from Fig. 4 that the square-shaped monopole is accountable for the generation of 1.95 GHz and 5.09 GHz frequency bands. Similarly, inverted L-shaped printed line is liable for the creation of 2.54 GHz frequency band. $TE^{x}_{\delta 11}$ and $TE^{y}_{1\delta 1}$ modal fields of rectangular DRA are accountable for the creation of 4.1 GHz frequency band. These resonances have also been confirmed theoretically in Section 2.

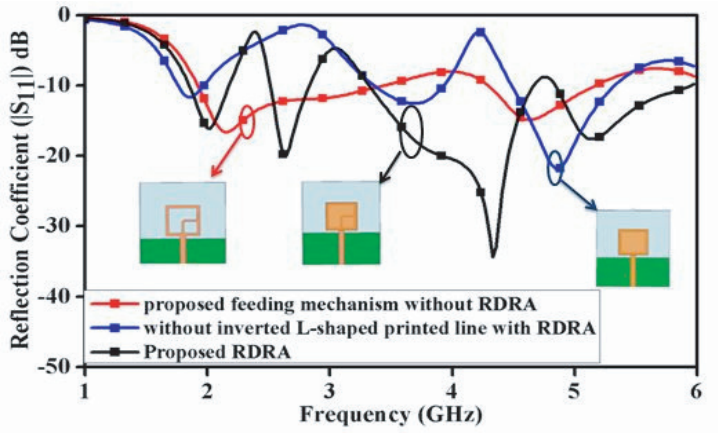

Figure 4. Reflection coefficient variation with and without RDRA and inverted L-shaped printed line.

E-field circulation on rectangular DRA at 4.0 GHz and 4.4 GHz is shown in Fig. 5. From near-field distribution, it is confirmed that the third frequency band (3.35 GHz–4.4 GHz) is the combined effort of dual orthogonal modes in RDRA ($TE^{x}_{\delta 11}$ and $TE^{y}_{1\delta 1}$) [14]. An inverted L-shaped printed line is used to

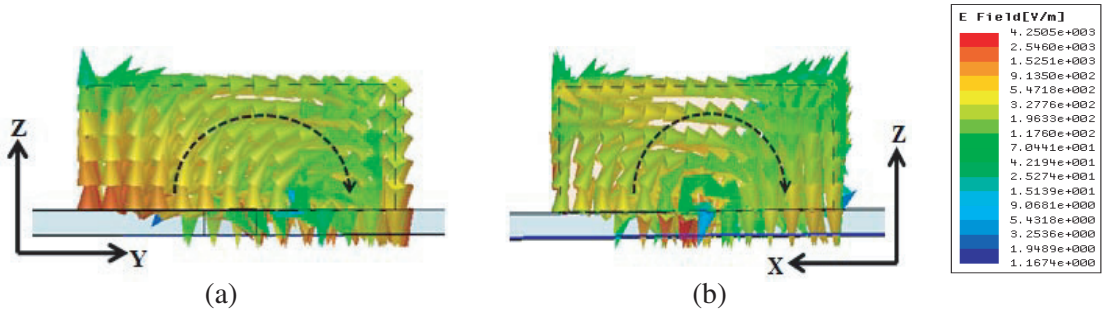

(a) (b)

Figure 5. Electric field distribution on rectangular DRA at (a) 4 GHz, (b) 4.4 GHz.

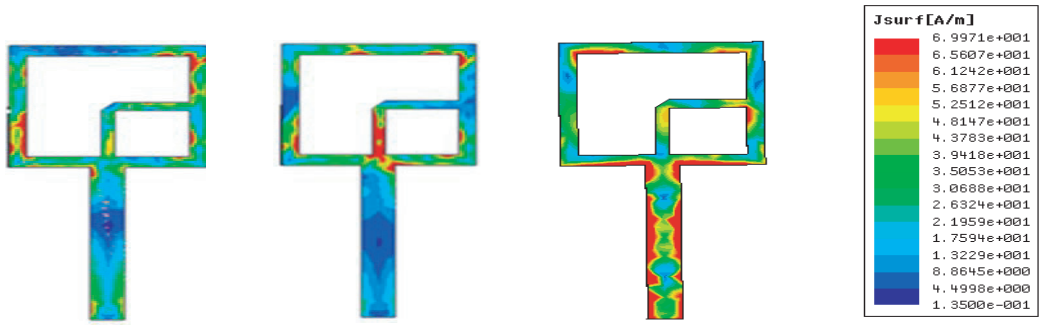

(a) (b) (c)

Figure 6. Surface current distribution on the modified square metallic ring at (a) 1.95 GHz, (b) 2.54 GHz, (c) 5.1 GHz.

create $\lambda/4$ path delay between the E-field lines of RDRA, which in turn create degenerated orthogonal modes ($TE^{x}_{\delta 11}$ and $TE^{y}1\delta 1$) in RDRA at 4.2 GHz.

Similarly, the current distribution on the surface of modified square metallic ring at 1.95 GHz, 2.54 GHz and 5.1 GHz is shown in Fig. 6. It is observed from Fig. 6 that square-shaped the metallic ring is responsible for 1.95 GHz and 5.1 GHz frequency bands because surface current is mainly concentrated over square-shaped ring at these two frequencies (1.95 GHz and 5.1 GHz). Similarly, at 2.54 GHz, the current is mainly concentrated over the inverted L-shaped printed line. Therefore, it can be said that the inverted L-shaped printed line is accountable for 2.54 GHz frequency band.

3.3. Generation of Circularly Polarized Wave

Axial ratio variation of the proposed radiator is shown in Fig. 7. In Fig. 7, we take three different cases: (1) square metallic ring along with inverted L-strip without RDRA; (2) square metallic ring along without inverted L-strip with RDRA; (3) proposed RDRA. It can be observed from Fig. 7 that axial ratio in the third frequency band (4.1–4.39 GHz) is generated due to orthogonal mode generation ($TE^{x}_{\delta 11}$ and $TE^{y}_{1\delta 1}$) in RDRA. 90° phase shift between x-and y-polarized E-field lines is generated by the inverted L-shaped printed line which is accountable for CP wave generation in the fourth frequency band (4.78–5.2 GHz).

4. EXPERIMENTAL RESULTS

It is mandatory to verify optimized simulated results with the help of practical measurement. This section of the presented article is focused on them too. Fig. 8 displays the comparison of measured and simulated reflection coefficients ($|S_{11}|$) of the proposed radiator. Reflection coefficient variation is measured with the help of vector network analyzer made by Rhode & Schwarz with Model No. ZVH 8

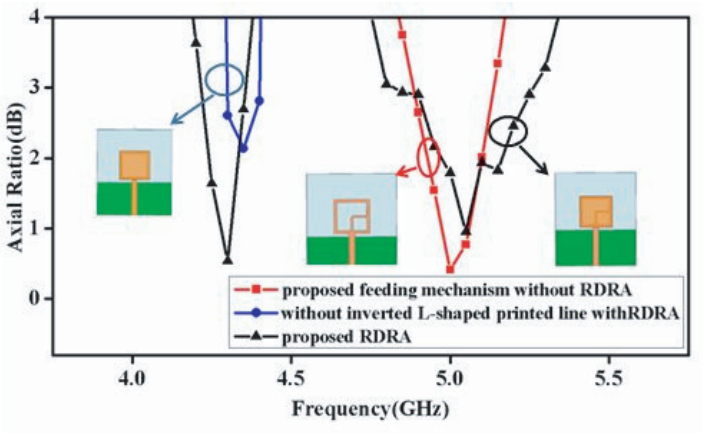

Figure 7. Axial ratio variation with different changes in proposed radiator towards ($\theta = 0$; $\varphi = 0$).

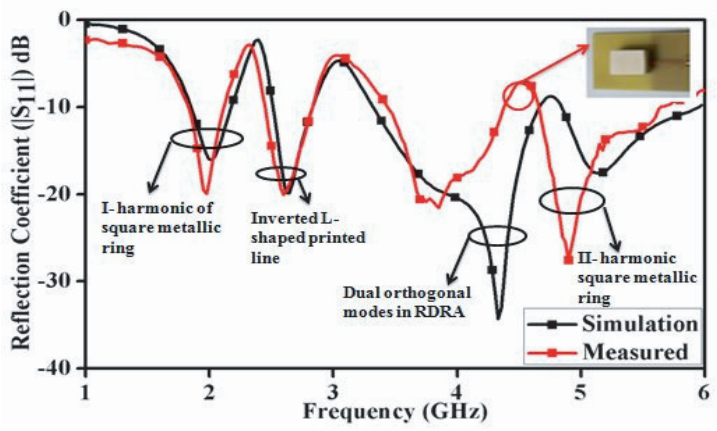

Figure 8. Experimental and simulated reflection coefficient variation of proposed radiator.

(100 kHz to 8.0 GHz). From Fig. 8, it is observed that there is good accordance between experimental and simulated outcomes. However, some differences are also observed due to fabrication errors such as use of adhesive material (quick fix) to fix the RDRA on the substrate [15].

Comparison between simulated and measured axial ratio variations of the proposed radiator towards broadside direction ($\theta = 0$; $\varphi = 0$) is shown in Fig. 9. Experimentally, axial ratio is measured with the support of dual linear pattern technique [16]. There is good agreement between measured and simulated axial ratio values. The measured 3-dB axial ratio bandwidths of lower and upper frequency bands are found to be 6.83% (4.1 GHz–4.39 GHz) and 8.41% (4.78 GHz–5.2 GHz), respectively. Assessment of

Table 2. Assessment of proposed radiator with existing dual band CP radiators on the basis of AR bandwidth.

Shape of Dielectric Resonator	Feeding Mechanism	Axial Ratio Bandwidth	
		Band-I	Band-II
Modified Rectangular [9]	Slot coupled	6.3%	3.68%
Cylindrical [10]	Coaxial probe	3.16%	5.06%
Chamfered [11]	Slot Coupled	5.2%	1.4%
Proposed Radiator	**Microstrip line**	**6.83%**	**8.41%**

the proposed radiator with additional existing antenna design on the basis of axial ratio bandwidth is exposed in Table 2. The proposed antenna structure has better axial ratio bandwidth in both the frequency bands. The proposed radiator uses rectangle-shaped DRA which can be easily available in the

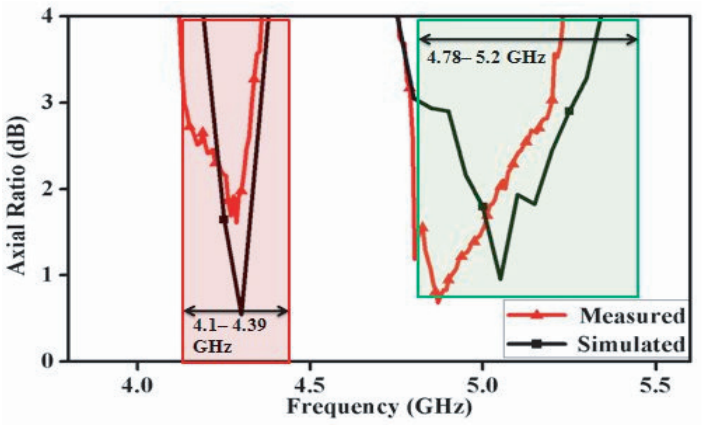

Figure 9. Experimental and simulated axial ratio variation of proposed radiator towards ($\theta = 0$; $\varphi = 0$).

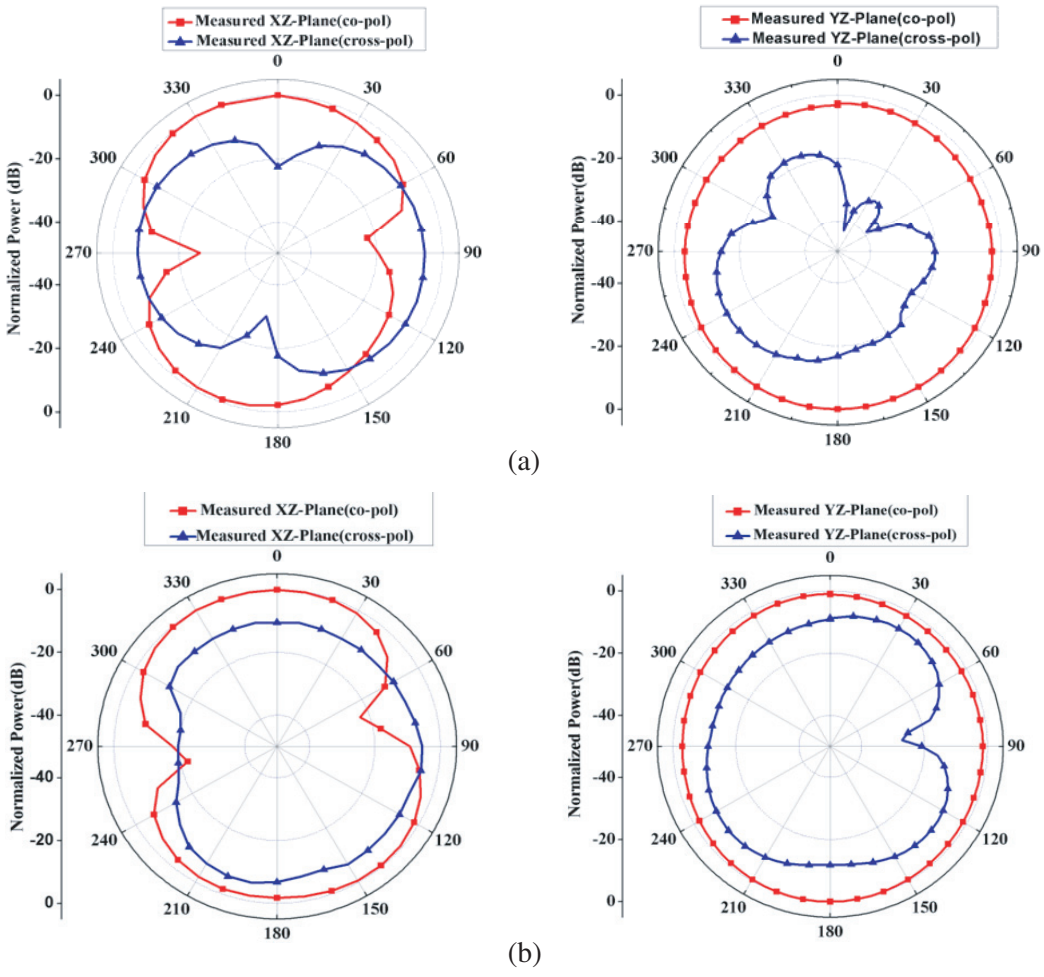

Figure 10. Measured XZ-plane and YZ-plane of proposed antenna at (a) 1.95 GHz, (b) 2.54 GHz.

commercial market. In a similar manner, microstrip line can be easily imprinted over an FR4 substrate, which makes the fabrication simpler than other published antenna structures.

Measured far-field patterns in two principle planes (XZ-plane and YZ-plane) at 1.95 GHz and 2.54 GHz are shown in Fig. 10. All these radiation patterns are measured in an automatic anechoic chamber. In linearly polarized frequency bands (1.95 GHz and 2.54 GHz), there is good co-pol to cross-pol difference towards the broadside direction ($\emptyset = 0°$, $\theta = 0°$), i.e., more than 15 dB. It is also observed that far-field pattern is dipolar in XZ-plane while it is omnidirectional in YZ-plane which confirms the monopole property of the proposed radiator. Similarly, LHCP and RHCP radiation patterns in two orthogonal planes (xz-plane and yz-plane) at 4.2 GHz and 4.85 GHz are displayed in Fig. 11. The proposed radiator shows LHCP pattern at 4.2 GHz because LHCP pattern is approx. 15 dB more than RHCP towards broadside direction. Similarly, at 4.85 GHz, it shows RHCP pattern because RHCP pattern is approx. 15 dB more than LHCP towards broadside direction. Fig. 12 displays the measured and simulated gains of the proposed radiator towards broadside direction ($\theta = 0$; $\varphi = 0$). Gain of the proposed radiator is measured with the help of two antenna method [1]. It is perceived from Fig. 12 that the gain value is larger in the frequency range where rectangular DRA radiates (3.35 GHz–4.4 GHz). The reason of higher gain is the nonappearance of metallic losses. The gain value is inferior in the fourth frequency band (4.62 GHz–5.62 GHz) to that in the first frequency band (1.81 GHz–2.06 GHz) because of the larger metallic losses at high frequency [1].

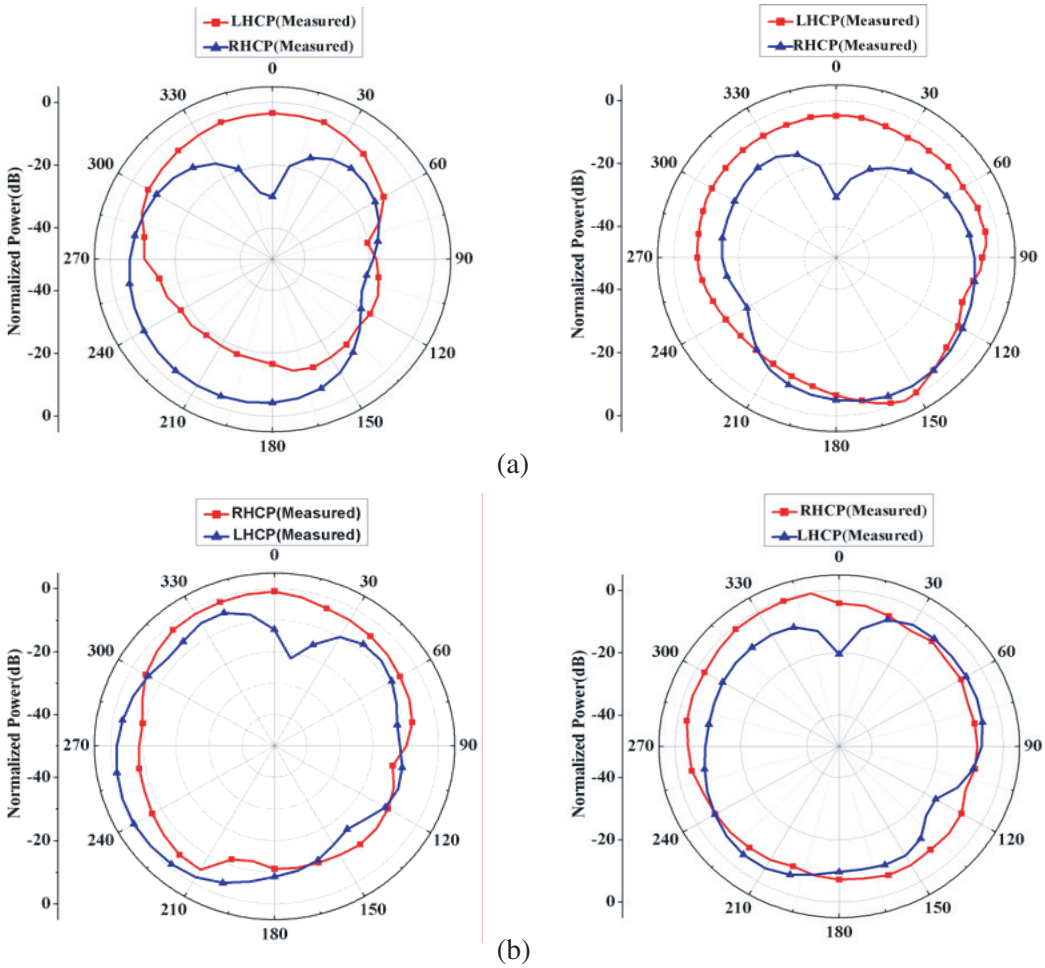

Figure 11. Measured LHCP and RHCP of proposed antenna in xz- and yz-plane at (a) 4.2 GHz, (b) 4.85 GHz.

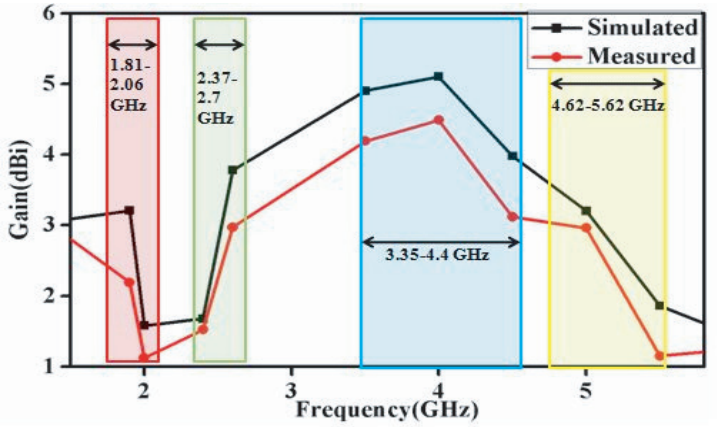

Figure 12. Measured and simulated gain versus frequency for proposed radiator towards ($\theta = 0$; $\varphi = 0$).

5. CONCLUSION

This paper presents a multiband composite dielectric resonator antenna configuration with dual-sense and dual-polarized characteristics. Out of four bands, first (1.81 GHz–2.06 GHz) and fourth frequency bands (4.62 GHz–5.62 GHz) are due to the first and second harmonics of square-ring monopole while second frequency band (2.37 GHz–2.7 GHz) is due to the inverted L-shaped printed line. Third frequency band (3.35 GHz–4.4 GHz) is the mutual endeavor of $TE^{x}_{\delta 11}$ and $TE^{y}_{1\delta 1}$ modes in rectangular DRA. Dual CP waves with different senses are generated due to the orthogonal modes in RDRA (4.1–4.39 GHz) and inverted L-shaped printed line (4.78–5.2 GHz). The proposed antenna is suitable for 3G bands (1.95 GHz), WiMAX (3.4/5.5 GHz) and WLAN (2.4 GHz) wireless applications.

ACKNOWLEDGMENT

Author, Ravi Kumar Gangwar wishes to acknowledge Science and Engineering Research board (SERB), DST, India, for financial support of this work through Young Scientist Scheme Project No. YSS/2014/000841.

REFERENCES

1. Balanis, C. A., *Antenna Theory: Analysis and Design*, 3rd edition, John Wiley & Sons, INC., Publication, New York, 2005.
2. Petosa, A., *Dielectric Resonator Antenna Handbook*, Artech House, Norwood, MA, USA, 2007.
3. Rao, Q., T. A. Denidni, and A. R. Sebak, "A new dual-frequency hybrid resonator antenna," *IEEE Trans. Antennas Propag.*, Vol. 4, 308–311, 2005.
4. Sharma, A. and R. K. Gangwar, "Triple band dual segment cylindrical dielectric resonator antenna with a novel microstrip feed for WLAN/WiMAX applications," *Microwave Opt. Technol. Lett.*, Vol. 57, 2649–2655, 2015.
5. Chen, H. M., Y. K. Wang, Y. F. Ling, S. C. Lin, and S. C. Pan, "A compact dual-band dielectric resonator antenna using a parasitic slot," *IEEE Antennas Wireless Propag. Lett.*, Vol. 8, 173–176, 2009.
6. Guha, D., P. Gupta, and C. Kumar, "Dual-band cylindrical dielectric resonator antenna employing $HEM_{11\delta}$ and $HEM_{12\delta}$ modes excited by new composite aperture," *IEEE Trans. Antennas Propag.*, Vol. 63, 433–438, 2015.
7. Sharma, A., P. Ranjan, and R. K. Gangwar, "Multiband cylindrical dielectric resonator antenna for WLAN/WiMAX applications," *IET Electronics Letter*, Vol. 53, 132–134, 2017.

8. Sharma, A. and R. K. Gangwar, "Circularly polarised hybrid Z-shaped cylindrical dielectric resonator antenna for multiband applications," *IET Microw. Antennas Propag.*, Vol. 10, 1259–1267, 2016.
9. Fang, X. and K. W. Leung, "Singly fed dual band circularly polarized dielectric resonator antenna," *IEEE Antennas Wireless Propag. Lett.*, Vol. 13, 995–998, 2016.
10. Pan, Y. M., S. Y. Zheng, and W. Li, "Dual-band and dual-sense omnidirectional circular polarized antenna," *IEEE Antennas Wireless Propag. Lett.*, Vol. 13, 706–709, 2014.
11. Ngan, H. S., X. S. Fang, and K. W. Leung, "Design of dual-band circularly polarized dielectric resonator antenna using a high-order mode," *Proc. IEEE-APS APWC*, 424–427, 2012.
12. Patel, P., B. Mukherjee, and J. Mukherjee, "Wideband circularly polarized rectangular dielectric resonator antennas using square-shaped slots," *IEEE Antennas Wireless Propag. Lett.*, Vol. 15, 1309–1312, 2016.
13. Pal, A., S. Behera, and K. J. Vinoy, "Design of multi-frequency microstrip antennas using multiple rings," *IET Microw. Antennas Propag.*, Vol. 3, 77–84, 2009.
14. Weng, Z., X. Wang, Y. Jiao, and F. Zhang, "Wideband rectangular Dielectric Resonator Antenna (DRA) with slot-fed design," *Progress In Electromagnetics Research Letters*, Vol. 16, 181–190, 2010.
15. Aras, M., M. Shahrieel, A. Aziz, and M. Z. Abidin, "Dielectric Resonator Antenna (DRA) for wireless application," *IEEE International RF and Microwave Conference Proceedings*, 454–458, Kuala Lumpur, Malaysia, 2008.
16. Stutzman, W. L. and G.'A. Thiele, *Antenna Theory and Design*, A John Wiley & Sons, INC., Publication, 2013.
17. Best, S. R., "The significance of ground-plane size and antenna location in establishing the performance of ground-plane-dependent antennas," *IEEE Antennas and Propag. Magazine*, Vol. 51, 29–43, 2009.